

# Multicompartment Polymer Vesicles with Artificial Organelles for Signal-Triggered Cascade Reactions Including Cytoskeleton Formation

Andrea Belluati, Sagana Thambo, Adrian Najer, Viviana Maffei, Claudio von Planta, Ioana Craciun, Cornelia G. Palivan,\* and Wolfgang Meier\*

Organelles, i.e., internal subcompartments of cells, are fundamental to spatially separate cellular processes, while controlled intercompartment communication is essential for signal transduction. Furthermore, dynamic remodeling of the cytoskeleton provides the mechanical basis for cell shape transformations and mobility. In a quest to develop cell-like smart synthetic materials, exhibiting functional flexibility, a self-assembled vesicular multicompartment system, comprised of a polymeric membrane (giant unilamellar vesicle, GUV) enveloping polymeric artificial organelles (vesicles, nanoparticles), is herein presented. Such multicompartment assemblies respond to an external stimulus that is transduced through a precise sequence. Stimuli-triggered communication between two types of internal artificial organelles induces and localizes an enzymatic reaction and allows ion-channel mediated release from storage vacuoles. Moreover, cytoskeleton formation in the GUVs' lumen can be triggered by addition of ionophores and ions. An additional level of control is achieved by signal-triggered ionophore translocation from organelles to the outer membrane, triggering cytoskeleton formation. This system is further used to study the diffusion of various cytoskeletal drugs across the synthetic outer membrane, demonstrating potential applicability, e.g., anticancer drug screening. Such multicompartment assemblies represent a robust system harboring many different functionalities and are a considerable leap in the application of cell logics to reactive and smart synthetic materials.


## 1. Introduction

The complex architecture of living cells, including simultaneous action of a myriad of dynamic processes, are the inspiration for creating sophisticated cell-like structures with the final goal of obtaining novel materials with cell-mimicking behaviors. Many aspects of living cells, including complex compartmentalization, energy transduction, signaling cascades, protein expression, growth and division, have been successfully modelled in isolation using artificial assemblies.<sup>[1]</sup> However, combining different cell functions while maintaining high spatiotemporal control remains challenging through the bottom-up assembly of synthetic and biological components. Another obstacle that needs to be overcome in the development of cell-mimicking materials is endowing them with the ability to dynamically modify their internal structure. In nature, cell mobility, shape, cell division, and intracellular transport rely on the dynamic assembly/disassembly of cytoskeletal components (e.g., actin) in combination with the action of motor proteins (e.g., myosin).<sup>[2]</sup> Repro-

duction of such a complex system that maintains the mobility, division, and transport seen within cells, is achievable using manmade autonomous artificial cells, however many hurdles remain.<sup>[1b]</sup>

Two common membranous structures utilized for building cell-like entities are either lipidic or polymeric giant unilamellar vesicles (GUV),<sup>[1a,d]</sup> with some reports of other systems such as proteinosomes, coacervates, colloidosomes, polypeptide, or polymer capsules.<sup>[3]</sup> Lipids, as natural components of cell membranes, are one of the most biocompatible building blocks for cell-like systems. However, issues with respect to stability and tuneability of lipid-based systems explains the great interest in synthetic polymer-based vesicles to overcome some of these challenges. Since the functionality of various membrane proteins can also be preserved when inserted in polymer membranes,<sup>[1a,4]</sup> the basis for creating complex cell-mimicking systems by combining synthetic and biological components is given. Key examples of cell mimics made from giant polymer

Dr. A. Belluati, Dr. S. Thambo, Dr. A. Najer,<sup>[†]</sup> Dr. V. Maffei, Dr. I. Craciun, Prof. C. G. Palivan, Prof. W. Meier  
Department of Chemistry  
University of Basel  
Mattenstrasse 24a, BPR 1096, Basel 4058, Switzerland  
E-mail: cornelia.palivan@unibas.ch; wolfgang.meier@unibas.ch  
C. von Planta  
Department of Chemistry  
University of Basel  
Klingelbergstrasse 80, Basel 4056, Switzerland

 The ORCID identification number(s) for the author(s) of this article can be found under <https://doi.org/10.1002/adfm.202002949>.

© 2020 The Authors. Published by WILEY-VCH Verlag GmbH & Co. KGaA, Weinheim. This is an open access article under the terms of the Creative Commons Attribution License, which permits use, distribution and reproduction in any medium, provided the original work is properly cited.

<sup>[†]</sup>Present address: Department of Materials, Imperial College London, South Kensington Campus, Prince Consort Road, London SW7 2AZ, UK

DOI: 10.1002/adfm.202002949

vesicles include demonstration of protein expression (actin monomer) via encapsulation of the whole expression machinery and building blocks,<sup>[5]</sup> energy production,<sup>[6]</sup> signal transduction via responsive subcompartments,<sup>[7]</sup> autonomous growth/blebbing/division,<sup>[8]</sup> and beating.<sup>[9]</sup>

With respect to cytoskeleton components inside artificial assemblies, actin polymerization has been mainly studied using giant liposomes to observe membrane transformations that underlay cell motility.<sup>[14]</sup> There are only two recent examples that address the complex mechanism of cytoskeleton formation inside artificial assemblies. In the first, microinjection of F-actin or polymerization during cell mimic formation using a lipid-based GUV system produced via microfluidics and the help of copolymer-stabilized water-in-oil droplets, was explored.<sup>[10]</sup> In the second, a more complex setup was demonstrated using a GUV system that successfully coupled photosynthesis and actin polymerization.<sup>[11]</sup> This last concept was recently evaluated on a nanoscale tubular polymersome system.<sup>[12]</sup> However, all of the cell-sized systems relied on the inherently less stable lipid-based membranes, and did not fully exploit the potentialities offered by a modular and stimuli-reactive system to mimic cells more in depth rather than focusing only on the formation of a cytoskeleton per se.

Subcompartmentalization of synthetic assemblies, much like organelles in living cells, can allow the localization of components and their hierarchical organization in discrete, sequential steps, changing their content and their internal structure. We recently reported a stimuli-responsive, cell-sized, polymer-based multicompartment system that can transduce a signal via triggerable subcompartments that in turn switch on an enzymatic reaction or deliver ion channels to the outer membrane permeabilizing it towards a secondary messenger.<sup>[7]</sup> Our system, based on micrometer-sized polymer vesicles with nanosized stimuli-responsive subcompartments, serves as the basis for cell mimics with more complex behaviors, to obtain advanced materials where internal organization can be dynamically changed upon a chemical stimulus. This bioinspired solution offers greater flexibility, compared to single-compartment systems, thanks to the intrinsic modularity of a hierarchical system containing different kinds of smaller, responsive subcompartments interacting with one another; additionally, the resulting compartmentalization influences positively the contained reactions and processes.<sup>[1a,13]</sup>

Here, we evolved our system to create a multicompartment smart material that contains structurally diverse compartments, which can transduce an external signal between two types of artificial organelles. With the addition of a cytoskeleton component (actin), such a system was able to form an internal cytoskeletal network (actin polymerization) via ion channel recruitment from the environment or even coloaded internal subcompartments. Using confocal microscopy, fluorescence correlation spectroscopy (FCS), and high-resolution fluorescence imaging (3D-SIM), we show that a complex signal transduction via a cascade involving two different types of artificial organelles can be achieved. Addition of the signaling molecule led to a signal transduction cascade that involves selective activation of the first types of artificial organelles to kick start either enzymatic reactions or channel recruitment to the secondary artificial organelle, producing a detectable compound

in the multicompartment's lumen/membrane. This setup was used as a system for triggered actin network formation within polymeric GUVs, which changed their content, on demand, in three ways i) by selective disassembly of subcompartments ii) by selective ion flow and iii) by cytoskeleton formation. This demonstration of precise temporal control over spatially confined components within a bottom-up cell mimic that performs complex sequential processes (a cascade, in a broad sense) upon applying a stimulus, opens up vast design options for various applications in fields such as catalysis, biosensing and biomedicine.

## 2. Results and Discussion

### 2.1. Coloaded of Polymer Vesicles and Nanoparticles as Subcompartments of GUVs

Due to the high stability of polymeric membranes,<sup>[4]</sup> the membrane of the microscale polymer GUVs were formed from a mixture of poly(2-methyl-2-oxazoline)<sub>5</sub>-*block*-poly(dimethylsiloxane)<sub>58</sub>-*block*-poly(2-methyl-2-oxazoline)<sub>5</sub> (PMOXA<sub>5</sub>-*b*-PDMS<sub>58</sub>-*b*-PMOXA<sub>5</sub>) and PDMS<sub>65</sub>-*b*-heparin copolymers, while loading of subcompartments was achieved simultaneously, using film rehydration technique in sucrose.<sup>[7]</sup> In the previous study we investigated the formation of one-type multicompartment, loading nanoparticles and heparin-nanostructures separately into GUVs (4–50 μm) which remained intact for at least six months.<sup>[7]</sup> To increase the complexity offered by such a modular system, we created two-type multicompartment, where two kinds of subcompartments, such as fluorescently labelled reduction sensitive nanoparticles (NP-Graft) and heparin-exposing polymer vesicles or micelles were simultaneously used as subcompartments of GUVs, forming two-type multicompartment (Figure 1A–C; Table S1, Supporting Information). The heparin nanostructures were composed of polymersomes formed from a mixture of PMOXA<sub>5</sub>-*b*-PDMS<sub>58</sub>-*b*-PMOXA<sub>5</sub> combined with PDMS<sub>65</sub>-*b*-heparin, and micelles resulting from pure PDMS<sub>65</sub>-*b*-heparin, while NP-Graft was based on the graft copolymer (poly(2-methyl-2-oxazoline)<sub>88</sub>-*graft*(SS)-poly( $\epsilon$ -caprolactone)<sub>238</sub> (PMOXA<sub>88</sub>-*g*(SS)-PCL<sub>238</sub>), whose disulfide bridge disconnects in a reductive environment, resulting in particle disassembly and PCL aggregation and precipitation.<sup>[14]</sup> The latter is thus the responsive subcompartment; NP-Graft can be loaded with several hydrophobic compounds (Table S1, Supporting Information).

The two-type multicompartment were first characterized by in situ FCS assisted by fluorescence confocal laser scanning microscopy (CLSM) to monitor the changes in diffusion time, corresponding size, and number of loaded subcompartments over time (Figure 1; Table S2, Supporting Information).<sup>[7]</sup> Additionally, we loaded two polymersome-based subcompartments (Ves5), each carrying a different fluorophore (Bodipy 630/650 and OG488), to visualize both compartments at once, with CLSM (Figure S1 and Table S1, Supporting Information).

The robustness of the detection system based on CLSM/FCS enables the evaluation of the cellular signaling transduction cascade. Using this technique, we can follow the selective cargo release from the reduction sensitive subcompartments

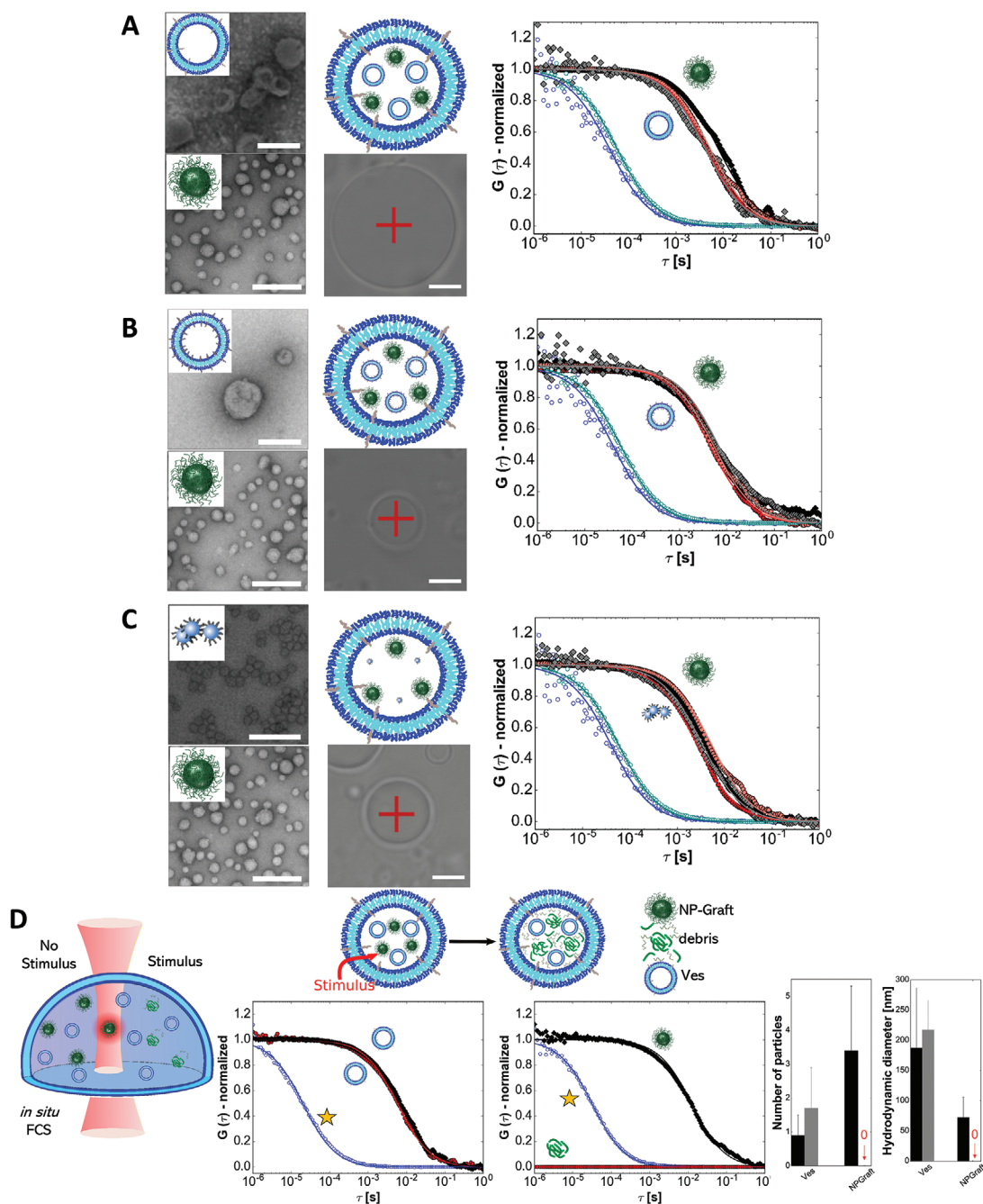


**Figure 1.** Characterization of multicompartments formed by loading GUVs with two different nanoassemblies (reduction-sensitive nanoparticles and nonreduction sensitive heparin nanostructures). TEM micrographs of each nanoassembly (left column), followed by a schematic illustration of multicompartments and their CLSM brightfield image. FCS measurement in combination with CLSM to quantify subcompartments inside giant vesicles (right column). FCS measurements: normalized autocorrelation curves are shown with symbols and the corresponding fits as solid lines. FCS measurements of the free dye (OG488 in blue, Bodipy630/650 in light blue), the nanoassemblies inside giant vesicles (OG488-loaded heparin nanostructures in black, Bodipy630/650-loaded NP-Graft in grey), and the free heparin nanostructures in solution (OG488 loaded heparin nanostructure in red, Bodipy630 loaded NP-Graft in light red) and Bodipy630 loaded NP-Graft in solution (light red), (right column). NP-Graft was coloaded with A) Ves5 (5%-Heparin vesicles), B) Ves25 (25%-Heparin vesicles), and C) M100 (100%-Heparin micelles) in giant vesicles. D) Characterization of the selective reduction sensitivity of two-type multicompartments (reduction-sensitive nanoparticles (NPGraft) and nonresponsive polymer vesicles (Ves)). Schematic illustration of multicompartment before and after addition of stimulus (DTT). The hydrodynamic diameter and number of particles (average in confocal volume) in the GUV show that in presence of DTT (grey) only the reduction sensitive NP-Graft disassembled, while the nonresponsive subcompartments (Ves) stayed intact. In absence of DTT, both subcompartments were stable (black) ( $N = 3$  GUVs before and after DTT per channel). For the FCS measurements: normalized autocorrelation curves are shown with symbols, corresponding fits as solid lines, measurements of the free dye in blue (Bodipy630/650), particles in absence of DTT (black) and after addition of DTT (red), incubation times 24 h. The yellow star represents free dye. Scale bars, 200 nm for TEM and 5  $\mu\text{m}$  for CLSM images.

(NP-Graft) in the presence of the membrane-permeating dithiothreitol (DTT), while simultaneously ensuring that the other subcompartments (Ves5) remain intact (Figure 1D). In absence of the stimulus, both subcompartments remained intact inside the lumen of the GUV:  $N = 3.4 \pm 1.9$  NP-Graft and  $N = 0.9 \pm 0.6$  Ves5 in the confocal volume. Considering the ratio between confocal and GUV volume, this corresponds to circa  $3780 \pm 740$  NP-Graft and  $1000 \pm 760$  Ves5 vesicles in an average  $1112 \pm 407 \mu\text{m}^3$  sized GUV,<sup>[7]</sup> meaning that NP-Graft occupy 0.2% of the GUV's volume, and the Ves5 3.1%. After a 24 h treatment with DTT, the reduction sensitive NP-Graft disassembled via disulfide bond cleavage, as seen by the disappearance of the correlation curve and a drop in the number of particles in the confocal volume to background levels (Figure 1D). The nonresponsive subcompartments preserved their architecture, confirming that the selective disassembly of only one subcompartment was successful. This set the basis for using this hierarchical assembly to create simple polymeric cell-mimicking vesicles with two subcompartments that act as artificial organelles performing cascade reactions triggered by an external signal.

## 2.2. Stimuli-Triggered Communication between Two Types of Internal Artificial Organelles

The responsive multicompartments were further upgraded by spatially segregating an enzyme from its substrate in two distinct artificial organelles. Upon arrival of a signal from the external medium, the enzymatic reaction should be triggered by recombining the substrate—released from within stimuli-responsive organelles—with enzymes entrapped within secondary organelles. The lipase substrate 1,2-Di-O-lauryl-rac-glycero-3-(glutaric acid 6-methylresorufin ester) (DGGR) was incorporated in the stimuli-responsive artificial organelle (NP-Graft) (Figure 2A; Table S1, Supporting Information). For the secondary artificial organelle, we entrapped the enzyme lipase in polymersomes (LipVes), with an adsorption efficiency of 73% (Figures S2 and S3, Supporting Information). Both artificial organelles were co-loaded into our polymer GUVs. No fluorescence was observed in a nonreductive environment, thanks to the spatial segregation of substrate and enzyme in the two organelles. Upon addition of the signaling molecule DTT to the GUVs, enzymatic substrate (DGGR) was released from the reduction sensitive subcompartment (NP-Graft) and free to interact with the enzyme in the secondary organelle (LipVes) forming the fluorescent product (methylresorufin) (Figure 2A,C; Figure S4, Supporting Information). The triggered enzyme activity was achieved in 90% of GUVs where methylresorufin either partitioned into the hydrophobic part of the GUVs membrane (ring-like fluorescence), or stuck to the hydrophobic part of the remaining subcompartments' membrane and NP-Graft debris in the lumen of the GUV, yielding a uniformly dispersed fluorescence (Figure S5, Supporting Information). 10% of the GUVs showed no fluorescence. In agreement with our previous report, DTT did not noticeably disrupt the enzyme and the confined reaction had additional dependence on the diffusion of DTT across the membrane and its reduction of the NP-Graft.<sup>[7]</sup> All traces of nonencapsulated LipVes present in solution were inactivated using Orlistat, a

lipase inhibitor. In conclusion, the lipase reaction inside the two-type multicompartments was successfully triggered by an external signal that induced a change in the internal architecture of the GUVs and released substrates reacted with the enzymes in the secondary organelles (LipVes). Even though the adsorption on vesicles did not change the overall activity of the enzyme, it affected the localization of the final product, with a significant fraction of the GUVs showing fluorescence in the lumen (35%, Figure S5, Supporting Information). In our previous study, we found more product located on the GUV's membrane when lipase was encapsulated in free form.<sup>[7]</sup> It must be noted that the GUVs had quite a broad size distribution with sizes between 4 and 29  $\mu\text{m}$ , a limitation of the film rehydration technique.

## 2.3. Reduction-Triggered Ion Release from Artificial Vacuoles

We further developed another two-type multicompartment system that, upon the reducing stimulus, transfers ion channels from one type of artificial organelles (NP-Graft) to secondary membranous artificial organelles acting as storage vacuoles ( $\text{Na}^+\text{Ves}$ ), hence permeabilizing them to allow the passage of stored monovalent cations (Figure 1C). For the on-demand release of sodium ions from the secondary storage organelle ( $\text{Na}^+\text{Ves}$ ), we co-loaded them in GUVs together with primary organelles (NP-Grafts) containing peptide gramicidin A (gA), known to form cation-permeable channels. Following the release of gA from the NP-Graft, the triggered recruitment of gA to the  $\text{Na}^+\text{Ves}$  was achieved via the externally added signaling molecule DTT (Figure 2B,D; Figure S6, Supporting Information). With gA immediately incorporated into the hydrophobic part of the membrane of the  $\text{Na}^+\text{Ves}$ , the sodium ions flowed from this artificial organelle into the GUV lumen, and there, activated the sodium sensitive dye Asante Natrium Green2 (ANG2). In addition, a fraction of gA inserted in the GUV membrane, since it is made of the same polymer. The surface offered to gA by the encapsulated  $\text{Na}^+\text{Ves}$  is roughly  $125 \mu\text{m}^2$  for the sum of the encapsulated polymersomes (1000 per GUV), versus  $452 \mu\text{m}^2$  for the membrane of a GUV (volume  $1112 \mu\text{m}^3$ ) would mean comparable recruitment to the artificial organelle membrane. We observed the increase in ANG2 fluorescence within the GUVs, which had a size distribution between 6 and 43  $\mu\text{m}$  ( $N = 40$  GUVs, Figure S7, Supporting Information), but could not observe any difference in kinetics compared to the case of insertion and ion flux across the GUV membrane due to gA insertion in GUVs membrane.<sup>[7]</sup> 73% of multicompartments were functional and induced the dye activation, via two types of artificial organelles coencapsulated within the GUVs. No fluorescence was detected in the remaining 27%, possibly due to insufficient loading of gA in NP-Graft, sodium ions in the  $\text{Na}^+\text{Ves}$ , subcompartments into GUVs, ANG2 into the GUVs, or a combination thereof (Figure S7, Supporting Information). As expected, the recruitment sequence did not occur in the absence of the stimuli DTT, showing no fluorescence. Our system was capable of triggering the recruitment of an ion channel from one organelle to another driving the flux of ions from the secondary organelle (storage vacuole), mimicking the flux of ions across organelles involved in several cell processes, such as signal transduction.<sup>[15]</sup>



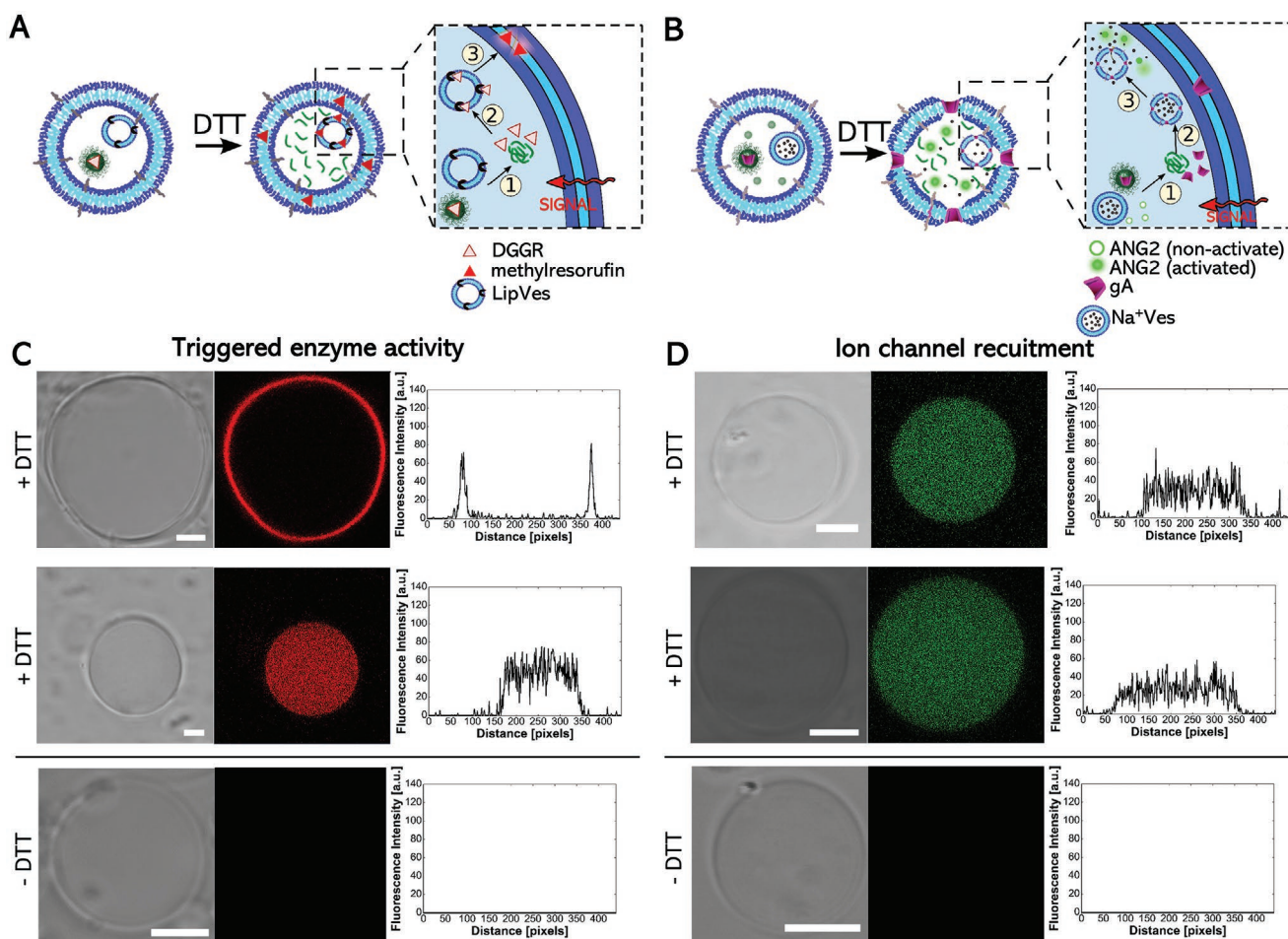


**Figure 2.** Characterization of the selective reduction sensitivity of two-type multicompartmental assemblies (reduction-sensitive nanoparticles (NP-Graft) and nonresponsive polymer vesicles (Ves)) for triggered enzyme activity and ion channel recruitment using two different internal subcompartments within GUVs. A) Schematic representation of enzymatic reaction using substrate (DGGR)-loaded NP-Graft and enzyme (lipase)-adsorbed polymersomes (LipVes), coloaded into GUVs. Substrate was released from NP-Graft in presence of DTT and transformed into the fluorescent product (methylresorufin). B) Schematic representation of gA mediated release of sodium ions from subcompartments. Upon the addition of DTT, encapsulated gA is released from its NP-Graft and inserts into the membrane boundary of the  $\text{Na}^+$  Ves and GUV. This allows sodium ions to exit the nano-sized vesicle cavity and to activate the sodium sensitive dye ANG2 in lumen of the GUV. C) CLSM imaging of DGGR loaded NP-Graft and LipVes in GUVs in presence (top, middle) and absence (bottom) of DTT. Bright field image (left), fluorescence image (center), and histogram along diagonal of fluorescence image (right). Due to the hydrophobicity of methylresorufin, it either partitioned into the hydrophobic part of the GUV's membrane or also to the remaining NP-Graft debris or nonresponsive LipVes membrane. D) CLSM imaging of gA loaded NP-Graft, sodium encapsulated polymersomes ( $\text{Na}^+$  Ves) and ANG2 co-loaded in GUVs in presence (top, middle) and absence (bottom) of DTT. Bright field image (left), fluorescence image (center) and histogram along diagonal of fluorescence image (right). The samples were incubated for 24 h. Scale bars, 5  $\mu\text{m}$ .

#### 2.4. Ion-Mediated Polymerization of Actin Inside GUVs

To explore the potential of our strategy to fabricate self-modulating multicompartmental assemblies, we first investigated the formation of an actin cytoskeleton, thus mimicking a basic component of cells responsible for both, structural stability and dynamic shape modifications. We encapsulated purified monomeric actin (G-actin) into our polymer-based GUVs, again by film rehydration and induced a selective permeability of the GUVs' membrane by entrapment of pore forming peptides and ion transporters, respectively (here named as ionophores). Upon addition of ions and their corresponding ionophores, such as ionomycin (IoNo) or gramicidin (gA) to the external medium, the GUV membrane becomes permeable to  $\text{Mg}^{2+}$

and  $\text{Ca}^{2+}$  (IoNo) or  $\text{K}^+$  ions (gA). The flux of ions successfully initiates actin polymerization inside the lumen of the multicompartment (Figure 3A). Ion-mediated actin filament formation is depended on the concentration and type of salts in its surrounding. This behavior depends on nonspecific interactions of actin cation binding sites, which are known to regulate biological functions such as cellular motility or shape and can also be replicated in nonliving liposomes.<sup>[1f,12,16]</sup>

We first confirmed fluorometrically the concentration ranges needed for polymerization with monomeric pyrene labeled actin in solution, showing formation of filaments in presence of various salt solutions ( $\text{KCl}$ ,  $\text{CaCl}_2$ , and  $\text{MgCl}_2$ ) (Figure S8, Supporting Information) at isosmotic concentrations. To enhance the creation of an ordered network, we mechanically stabilized our

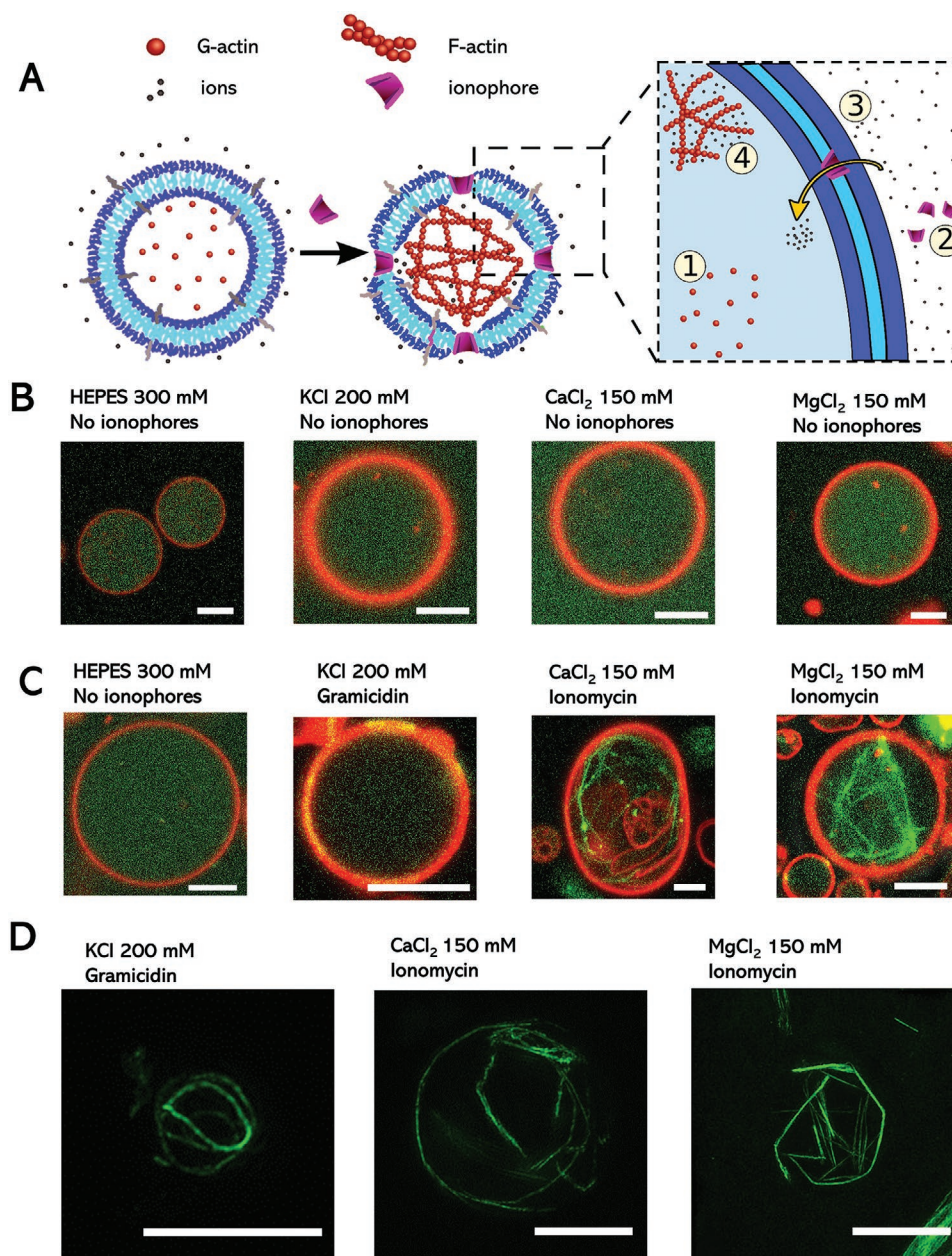


**Figure 3.** Actin filament polymerization in synthetic GUVs. Actin monomers (G-actin) and the actin crosslinker filamin was loaded into giant vesicles after 24 h incubation. Ionophores such as the channel *gA* or the organic molecule *IoNo* were introduced to the vesicle solution resulting in permeabilization of the GUV membrane towards specific ions ( $K^+$  or  $Ca^{2+}$  and  $Mg^{2+}$ ). A) Schematic representation of the actin polymerization in GUVs. B) In absence of ionophores, the monomers stayed intact and no filaments were formed since no ions could enter the GUV cavity. C) When ionophores were added to the surrounding solution, they reconstituted into the membrane boundary of the GUV (red). When ions enter the GUV cavity, actin starts to form filaments and the bundling agent filamin crosslinks the filaments into a network (green). D) Projections of actin filaments (green) polymerized in GUVs in presence of ionophores (*gA*, *IoNo*) and ions ( $K^+$ ,  $Ca^{2+}$ ,  $Mg^{2+}$ ) recorded with super-resolution 3D structured illumination microscopy (3D-SIM). The actin samples were incubated for 24 h. Scale bars, 5  $\mu$ m.

actin cytoskeleton (visualized with ATTO488-G-actin added to it) with the actin-binding protein filamin, which also helped the visualization of the filament networks,<sup>[17]</sup> which we could observe in ion-rich HEPES solutions (Figure S9, Supporting Information). We then proceeded to load the proteins into the GUVs (actin GUVs), yielding results (Figure 3C) qualitatively consistent with the data published earlier in liposomes loaded with actin

bundles.<sup>[16d,18]</sup> The hydrophobic Bodipy630/650 was used to visualize the GUV membrane. For future functionalization purposes, we also incorporated azide-modified PMOXA-PDMS-PMOXA during GUV formation, to allow simple click-chemistry conjugation of several species, such as dibenzocyclooctine-containing moieties, as demonstrated with a fluorescent model compound conjugated after self-assembly (Figures S10 and S11, Supporting

Information). As shown by CLSM (Figure 3B), in absence of ionophores and/or salts the actin monomers remained in their monomeric form within the GUVs (no observed filaments). When ionophores and salts were added to the outside of actin GUVs, filaments were formed within 24 h, in 88.5% of the vesicles ( $N = 200$  GUVs) (Figure 3C; Figures S12 and S13, Supporting Information), thanks to the diffusion of  $K^+$  through membrane-inserted gA, or  $Mg^{2+}/Ca^{2+}$  through IoNo. The shapes of the formed filaments were similar, regardless of the salts. Actin filaments formed either ring-like structures directly underneath the GUV membrane (inner leaflet), following the round membrane by bending the actin filaments, or formed web-like network structures within the GUV cavity.

To better visualize the morphology of the GUV cytoskeleton, we additionally used a high resolution microscopy technique, 3D structured illumination microscopy (3D-SIM), showing that the actin network within the GUVs is composed of both thin actin filaments and actin bundles with thicker fibers (Figure 3D). In most cases, when actin polymerized, we observed networks of actin within the GUVs and ring-like formations underneath the membrane. This is due to the vesicular morphology of our multicompartments that usually forces the polymerized actin to organize into cortical rings or web-like construct, minimizing the energy cost associated with bending of filaments, as demonstrated in lipid-based systems.<sup>[16d]</sup> As we did not observe any filaments formed by nonencapsulated actin, when tested with the same salts and actin concentrations present in the surrounding of GUVs, we conclude that any actin not encapsulated during the GUV formation process would be below the critical concentration of actin needed for polymerization to occur (Figure S14, Supporting Information). Therefore, no further removal of unencapsulated actin was necessary prior to imaging. Our observations confirmed that we could successfully trigger salt-induced actin polymerization in polymeric GUVs via addition of ionophores.

## 2.5. Triggered Actin Polymerization in GUVs through a Signaling Cascade

Aiming at increasing the complexity of our polymer-based cell mimics, we combined triggerable artificial organelles with cytoskeleton components to achieve signal-induced cytoskeleton formation inside the vesicle with the first signal being transduced via responsive subcompartments (“actin MCs”). The actin filaments should only form in the presence of an externally added signal that acts on the stimuli-responsive artificial organelle. Upon release of ion channels from these artificial organelles and inside-out insertion into the GUV membrane, ion influx from the environment should trigger actin polymerization (Figure 4A). Reduction sensitive subcompartments (NP-Graft), loaded with either gA or IoNo, were encapsulated in GUVs together with actin monomers and filamin. Actin stayed monomeric within the GUV in the absence of the signal (DTT), ions, or both signal and ions (Figure 4B; Figure S15, Supporting Information). In presence of DTT, the ionophore-loaded NP-Graft disassembled and released their cargo. As already observed with the addition from the outside, gA or IoNo incorporated into the GUV membrane allowing the

passage of  $K^+$ ,  $Mg^{2+}$  or  $Ca^{2+}$  through the membrane from the exterior solution, leading to the polymerization of actin in the GUV (Figure 4C–E; Figures S16 and S17, Supporting Information). Observations of mostly cortical rings in the case of triggered actin polymerization via responsive artificial organelles (Figure 3) could be due to a lower amount of gA or IoNo incorporated into the membrane compared to addition from the outside, as it depends on the loading and subsequent release from subcompartments (Graft-NPs). Limited amount of ion influx could lead to a more localized actin polymerization directly below the membrane where the local concentration of ions will be highest upon channel insertion. This explanation is also suggested by the fact that addition of ionophores from the outside (Figure 3) allows fast and plentiful influx of ions that leads to a higher probability of creating extended networks within the lumen, whereas the actin rings below the membrane are also present in the cases of increased ion influx (Figure 3D). Such mechanistic considerations will need to be further investigated in the future.

In absence of actin, the GUVs were spherical (Figure S18, Supporting Information) and impermeable, likewise when loaded with monomeric actin (1% nonspherical shape,  $N = 200$  GUVs) (Figures 3B and 4B). The actin filaments spanned several  $\mu\text{m}$  vertically, showing a cytoskeleton developing in various shapes within the GUV (Figure S19, Supporting Information). Permeabilization mainly conserved the spherical shape, but we also observed membrane deformations, due to the bundled up confined filaments (28.5%,  $N = 200$  GUVs) (Figures S20 and S21, Supporting Information).

Previous studies have revealed such changes in morphology with actin filaments in lipid structures, including protruded shapes, where the driving force for membrane deformations (elongation, contractions and protrusion) is generated in crowded condition in the compartment, as in living cells.<sup>[16d,19]</sup> Lipid membranes are known to be fluid-like and easily deformable compared to polymeric membranes that are less fluid/deformable when the membrane is thicker than the lipidic one.<sup>[20]</sup> The mechanical stress of actin filaments make giant liposomes more deformable and less stable;<sup>[19]</sup> our synthetic actin-GUVs were stable for at least 48 h, thanks to the higher stability of the polymer membrane. Stiffer actin bundles, formed due to higher filamin concentration, remain straight resulting in elongation of the vesicular structures or even puncturing the membrane due to inability to bend the actin bundles.<sup>[16d]</sup> Also in nature, the membrane tension of cells acts as a regulator of cytoskeleton architecture.<sup>[21]</sup> This behavior was more evident when gA or IoNo were added from the outside, i.e., without the DTT-induced release from subcompartments, probably due to partial reduction and denaturation of filamin by DTT, thus decreasing the bundle thickness.<sup>[22]</sup> On occasion, the stiff filaments pierced through the polymeric membrane and connected polymer compartments (Figure S21, Supporting Information), sometimes even connecting actin protrusions along the inner leaflet between GUVs (Figures S22 and S23, Supporting Information).

The cytoskeleton, as a molecular crowding agent, increases the internal viscosity of cells;<sup>[23]</sup> thus, we employed in situ FCS measurements to study the viscosity changes inside our actin MCs due to triggered actin polymerization. We used GUVs filled with responsive ionophores loaded artificial organelles



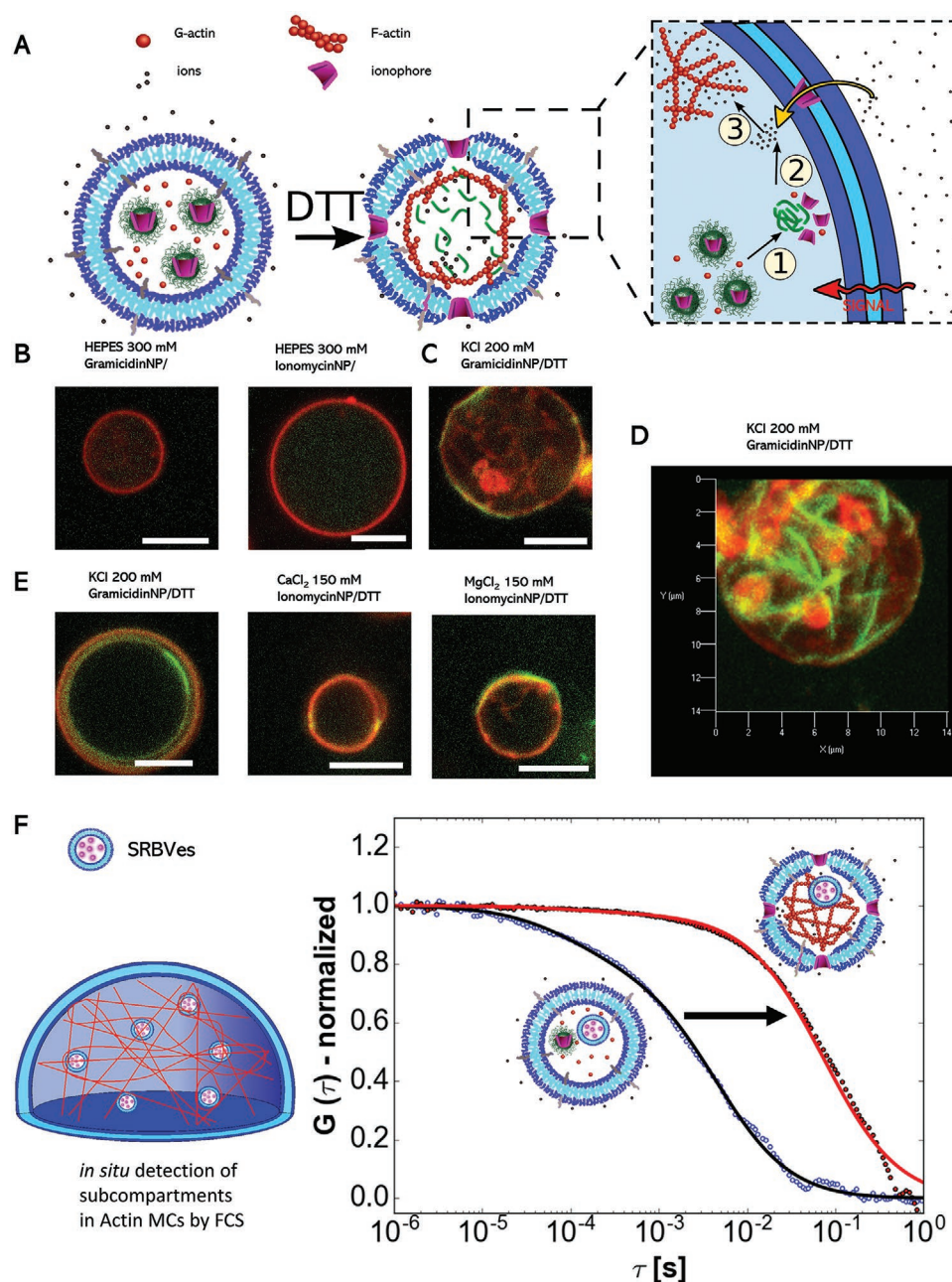


**Figure 4.** Stimuli-triggered actin polymerization in synthetic multicompartment vesicles (“actin MCs”). A) Schematic representation of ion import inducing selective membrane permeabilization that results in the formation of actin filaments. Upon DTT addition, the encapsulated ionophores are released from its NP-Graft and inserts into the GU membrane boundary. Ions enter from the surrounding solution into the cavity of the GU, where the actin monomers start to polymerize into filamentous structures. B) CLSM imaging of actin monomer (G-actin, green) and crosslinker filamin coloaded GUVs (red) remaining in its monomeric form in absence of salts and ionophores. C) One slice of Figure 3D. Actin filaments (green) and GU membrane (red), where actin polymerization is induced in presence of DTT. D) Projections of actin filaments (green) in GUVs (red) via stimuli responsiveness via internal subcompartments, were imaged with CLSM. The actin samples were incubated for 24 h. Each single slice is shown in Figure S17 in the Supporting Information. Scale bars, 5  $\mu\text{m}$ . E) CLSM micrographs of actin filaments (green) in the lumen and inner leaflet of the GU membrane (red), where actin polymerization is induced in presence of DTT. F) FCS autocorrelation curve of SRBVs of two-type multicompartment vesicles before and after triggered actin filament polymerization. Change in diffusion time can be indicated as viscosity change. ( $N = 3$  GUVs before and after addition of DTT).

(IoNo-loaded NP-Graft) and nonresponsive fluorescent subcompartments (SRBVs), plus actin and filamin. We measured the diffusivity of the labelled nonresponsive subcompartments (SRBVs) before and after selective disassembly of NP-Graft by adding DTT and subsequent formation of

filaments after ion influx. Based on the change in SRBVs diffusion times from 4555 to 70 277  $\mu\text{s}$  of otherwise unchanged vesicles, we could calculate a change of internal dynamic viscosity from  $1.3 \times 10^{-3}$  Pa s (viscosity of  $300 \times 10^{-3}$  M sucrose) to  $1.4 \times 10^{-2}$  Pa s after polymerization, yielding a relative viscosity



$\eta_r = 10.51$ . The actin filaments within the GUV made the lumen more crowded, replicating the molecular crowding of cells (Figure 4F). We successfully demonstrated that polymeric membranes and the actin biopolymers regulate each other's conformation in a force balance, where the membrane acts as barrier for selective diffusion of molecules, and frames actin bundles, which in turn influence the membrane shape. The actin component in our multicompartiment system, combined with functional artificial organelles, provides a complex and highly controlled active material, a step forwards bringing us closer to mimicking the complex mechanisms involved in cellular movement, shape, cell division, and intracellular transport.

We then performed a complete morphology analysis. Regarding the shape of the cytoskeleton, we could remark that web-like structures were the main type for actin GUVs (between 71% and 92%). In contrast, formation of cortical actin rings was predominantly observed for actin MCs (between 75% and 80%,  $N = 100$  GUVs) (Figure 5A,B). The shape of nonspherical actin MCs was also analyzed: the biggest population was represented by elongated vesicles (38%), then vesicles connected through

tubular protrusions of their nonruptured membranes ("beads on a string") and finally round vesicles showing long protrusions ( $N = 60$  GUVs) (Figure 5C). All these shapes were formed by underlying cortical actin rings. Various parameters such as concentrations of actin, filamin, ions, ionophores, stiffness of the membrane and of the filaments and more, influence the overall shape of the GUVs, which will have to be studied in more detail to depict the mechanism by which these structures are formed and how they dynamically change over time.

## 2.6. The Influence of the Membrane on the Diffusion of Polymerization Inhibitors

Actin polymerization is the main target of several natural compounds, which exert their toxic activity by inhibiting the polymerization of actin, which leads to aberrations in cell transport, motility and division.<sup>[24]</sup> Such natural toxins are candidate cytoskeletal drugs, as their interaction with actin can be a way to inhibit cell proliferation, making them anticancer agents, or

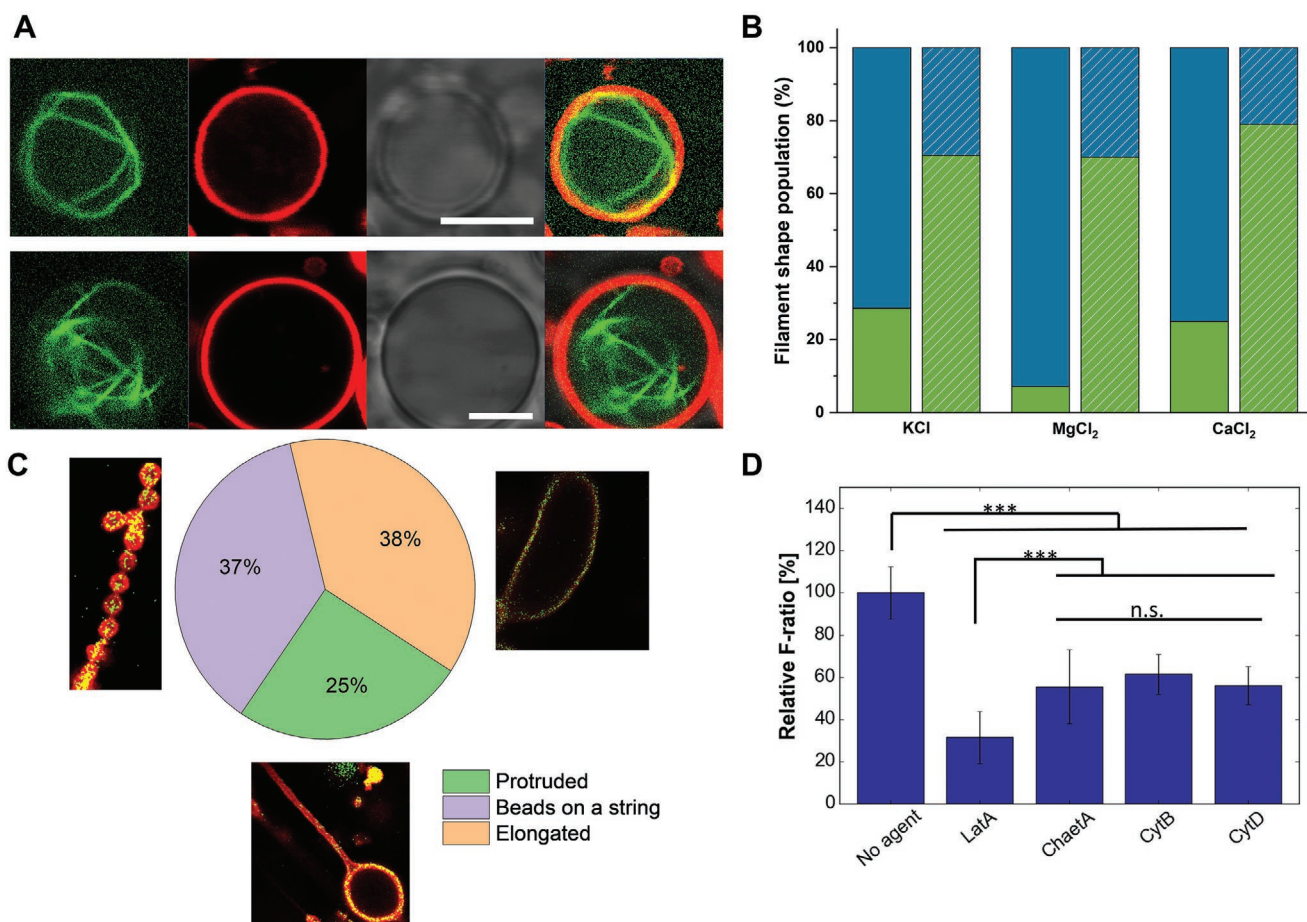


**Figure 5.** Analysis of actin filament shapes, GUV shapes and the effect of actin polymerization inhibitors on Actin MCs. A) An actin GUV with a cortical ring cytoskeleton. B) Bar graph showing filament shape frequency for actin GUVs (solid color) and actin MCs (striped color), in presence of different salts. Green: cortical rings, blue: web-like networks. The population of cortical rings increases noticeably in actin MCs ( $N = 100$ ). C) Shape distribution of nonspherical Actin MCs, showing a prevalence of elongated vesicles with cortical rings, closely followed by bead-like structures and then vesicles with protrusions ( $N = 60$ ). D) Relative F-ratio of untreated Actin MCs (set as 100%) and MCs treated with different toxins. The F-ratio determines how much a molecule can hinder the polymerization of actin. Error bars given as Mean  $\pm$  SD (binomial distribution),  $n$  between 15 (ChaetA) to 55 (CytD). Values compared through one-way ANOVA, with Tukey's post hoc test. \*\*\*  $p < 0.001$ ; n.s. not significant. Scalebar, 5  $\mu$ m.

biopesticides.<sup>[25]</sup> These toxins have different potency, meaning that the concentrations needed to achieve an effect can vary due to various uptake mechanisms and interactions with other cellular targets.<sup>[25b]</sup> An important factor to consider, when studying cytoskeletal drugs, is whether they rely on passive diffusion or transporters;<sup>[26]</sup> additionally, secondary targets for the toxins in cells must be accounted for when characterizing their interaction with actin, as the observed cytotoxicity might derive also from other interactions.<sup>[25a]</sup>

Our system can be used as a cytoskeletal drug screening platform to study the inhibitory action of small molecule actin-polymerization inhibitors. This system developed by narrowing down “cells” into two components: a cell-mimicking membrane, through which molecules can only passively diffuse, and a cytosol-mimicking lumen containing actin, will allow us to study the direct effect of the drugs on mechanical properties of cell-like systems.<sup>[27]</sup> To test such an application, we induced actin polymerization through DTT-triggered release of ionomycin from NP-Graft and flow of Mg<sup>2+</sup> in presence and absence of externally added actin polymerization inhibitors. As a proof of concept, we tested four different toxins, all membrane-permeable: latrunculin A (LatA), chaetoglobosin A (ChaetA), cytochalasin B (CytB), and cytochalasin D (CytD). The simultaneous addition of one of four toxins meant that the DTT-triggered actin polymerization had to compete with the compounds, which had in turn to diffuse across the polymer membrane. All screened compounds were added at the same concentration, above their reported EC<sub>50</sub>,<sup>[28]</sup> so that the only discriminants would be their ability to cross the membrane, and their intrinsic activity. All toxins showed significant ability of reducing what we called relative F-ratio, the ratio between GUVs presenting at least one filament and the total population, compared to the untreated MCs. We observed the highest effect with LatA, known to be one of the most potent polymerization inhibitors.<sup>[29]</sup> We found no significant differences between Chaet A, CytB, and CytD. These results suggest that the differences in potency between the compounds could partially be explained by their ability to diffuse through membranes, in addition to their intrinsic activity (Figure 5D). ChaetA was a remarkable case, as its addition led to the disassembly of a great number of vesicles (Figure S24, Supporting Information), hinting that it interacts with both the membrane and actin, which could be a future research direction to elucidate its toxic action in biological settings. We envision that finding polymerization inhibition in our system is an indicator of potential toxicity of the compound, since the compound could act on many different cells in the body through passive diffusion across the membrane. Interesting drug candidates would be inhibitors of actin polymerization in solution, but present no activity in our system. Such compounds could potentially be delivered to cancer cells specifically using targeted nanocarriers. Our findings present a possible application of our system, to screen for specific parameters affecting the action of compounds of pharmacological interest.

### 3. Conclusions

In conclusion, we demonstrated that our hybrid protein-polymer cell-like system is a responsive multicompartment

platform able to modify, selectively and following a chemical stimulus, its internal structure and content, mimicking aspects of cell behavior. These changes included triggered enzymatic activity, controlled membrane permeability, and cytoskeleton formation, achieving a self-contained and self-regulating responsive material, which can change its internal architecture and content with a complex tunable series of sequential steps. This complex and bio-inspired construct is a promising platform for the development of smart materials, sensing external factors and responding accordingly, with potential applications in biosensing and theranostics. As a first proof of concept, we showed how we could differentiate the influence of cross-membrane diffusion of different actin polymerization inhibitors. Future research will aim at using less potent reducing agents (e.g., GSH), which will require insertion of additional membrane proteins to permeabilize the polymeric membrane for such molecules.<sup>[30]</sup> The lack of control over the size distribution of multicompartment will be improved with the adoption of a microfluidic-based assembly approach.<sup>[31]</sup> We envision that the reported strategy has the potential to include even more complex functionalities by exchanging the trigger (signaling molecules), subcompartments (artificial organelles), and surface components to progress towards creation of an artificial cell.

### Supporting Information

Supporting Information is available from the Wiley Online Library or from the author.

### Acknowledgements

A.B. and S.T. contributed equally to this work. The authors acknowledge financial support from the Swiss National Science Foundation, NCCR-MSE, and University of Basel. The authors are grateful to Gabriele Persy for TEM imaging, Dr. Alexia Loynton-Ferrand (IMCF, University of Basel) for 3D-SIM imaging, Sven Kasper, and Dr. Dalin Wu for the synthesis of polymers.

### Conflict of Interest

The authors declare no conflict of interest.

### Keywords

artificial organelles, biomimetic actin cytoskeleton, signalling pathways mimics, stimuli-responsive multicompartment systems, synthetic giant vesicles/polymersomes

Received: April 2, 2020

Revised: April 30, 2020

Published online:

[1] a) A. Belluati, I. Craciun, C. E. Meyer, S. Rigo, C. G. Palivan, *Curr. Opin. Biotechnol.* **2019**, *60*, 53; b) K. Göpfrich, I. Platzman, J. P. Spatz, *Trends Biotechnol.* **2018**, *36*, 938; c) H. Jia, P. Schwillie,

- Curr. Opin. Biotechnol.* **2019**, *60*, 179; d) E. Rideau, R. Dimova, P. Schwiller, F. R. Wurm, K. Landfester, *Chem. Soc. Rev.* **2018**, *47*, 8572; e) T. Trantidou, M. Friddin, Y. Elani, N. J. Brooks, R. V. Law, J. M. Seddon, O. Ces, *ACS Nano* **2017**, *11*, 6549; f) N. A. Yewdall, A. F. Mason, J. C. M. van Hest, *Interface Focus* **2018**, *8*, 20180023; g) C. Love, J. Steinkühler, D. T. Gonzales, N. Yandrapalli, T. Robinson, R. Dimova, T. Y. D. Tang, *Angew. Chem., Int. Ed.* **2020**, *59*, 5950; h) A. F. Mason, N. A. Yewdall, P. L. W. Welzen, J. Shao, M. van Stevendaal, J. C. M. van Hest, D. S. Williams, L. K. E. A. Abdelmohsen, *ACS Cent. Sci.* **2019**, *5*, 1360; i) J. W. Hindley, Y. Elani, C. M. McGilvery, S. Ali, C. L. Bevan, R. V. Law, O. Ces, *Nat. Commun.* **2018**, *9*, 1093.
- [2] L. Blanchoin, R. Boujemaa-Paterski, C. Sykes, J. Plastino, *Physiol. Rev.* **2014**, *94*, 235.
- [3] X. Huang, M. Li, D. C. Green, D. S. Williams, A. J. Patil, S. Mann, *Nat. Commun.* **2013**, *4*, 2239.
- [4] C. G. Palivan, R. Goers, A. Najer, X. Zhang, A. Car, W. Meier, *Chem. Soc. Rev.* **2016**, *45*, 377.
- [5] C. Martino, S.-H. Kim, L. Horsfall, A. Abbaspourrad, S. J. Rosser, J. Cooper, D. A. Weitz, *Angew. Chem., Int. Ed.* **2012**, *51*, 6416.
- [6] L. Otrin, N. Marušič, C. Bednarz, T. Vidaković-Koch, I. Lieberwirth, K. Landfester, K. Sundmacher, *Nano Lett.* **2017**, *17*, 6816.
- [7] S. Thamboo, A. Najer, A. Belluati, C. von Planta, D. Wu, I. Craciun, W. Meier, C. G. Palivan, *Adv. Funct. Mater.* **2019**, *0*, 1904267.
- [8] B. P. Bastakoti, J. Perez-Mercader, *Adv. Mater.* **2017**, *29*, 1704368.
- [9] R. Tamate, T. Ueki, R. Yoshida, *Adv. Mater.* **2015**, *27*, 837.
- [10] M. Weiss, J. P. Frohnmayer, L. T. Benk, B. Haller, J.-W. Janiesch, T. Heitkamp, M. Börsch, R. B. Lira, R. Dimova, R. Lipowsky, E. Bodenschatz, J.-C. Baret, T. Vidaković-Koch, K. Sundmacher, I. Platzman, J. P. Spatz, *Nat. Mater.* **2017**, *17*, 89.
- [11] K. Y. Lee, S.-J. Park, K. A. Lee, S.-H. Kim, H. Kim, Y. Meroz, L. Mahadevan, K.-H. Jung, T. K. Ahn, K. K. Parker, K. Shin, *Nat. Biotechnol.* **2018**, *36*, 530.
- [12] S. Dhir, S. Salahub, A. S. Mathews, S. K. Kumaran, C. D. Montemagno, S. Abraham, *Chem. Commun.* **2018**, *54*, 5346.
- [13] N. Ichihashi, T. Yomo, *Curr. Opin. Chem. Biol.* **2014**, *22*, 12.
- [14] A. Najer, D. Wu, M. G. Nussbaumer, G. Schwertz, A. Schwab, M. C. Witschel, A. Schäfer, F. Diederich, M. Rottmann, C. G. Palivan, H.-P. Beck, W. Meier, *Nanoscale* **2016**, *8*, 14858.
- [15] H. Xu, E. Martinoia, I. Szabo, *Cell Calcium* **2015**, *58*, 1.
- [16] a) K. Carvalho, F.-C. Tsai, E. Lees, R. Voituriez, G. H. Koenderink, C. Sykes, *Proc. Natl. Acad. Sci. USA* **2013**, *110*, 16456; b) H. Kang, M. J. Bradley, W. A. Elam, E. M. De La Cruz, *Biophys. J.* **2013**, *105*, 2621; c) E. Loiseau, J. A. M. Schneider, F. C. Keber, C. Pelzl, G. Massiera, G. Salbreux, A. R. Bausch, *Sci. Adv.* **2016**, *2*, e1500465; d) F.-C. Tsai, G. H. Koenderink, *Soft Matter* **2015**, *11*, 8834.
- [17] A. J. Sutherland-Smith, *Biophys. Rev.* **2011**, *3*, 15.
- [18] a) T. Luo, V. Srivastava, Y. Ren, D. N. Robinson, *Appl. Phys. Lett.* **2014**, *104*, 153701; b) E. Schäfer, M. Vache, T.-T. Kliesch, A. Janshoff, *Soft Matter* **2015**, *11*, 4487.
- [19] S. Tanaka, K. Takiguchi, M. Hayashi, *Commun. Phys.* **2018**, *1*, 18.
- [20] F. Itel, M. Chami, A. Najer, S. Lörcher, D. Wu, I. A. Dinu, W. Meier, *Macromolecules* **2014**, *47*, 7588.
- [21] P. Sens, J. Plastino, *J. Phys.: Condens. Matter* **2015**, *27*, 273103.
- [22] a) R. C. Page, J. G. Clark, S. Misra, *Acta Crystallogr., Sect. F: Struct. Biol. Cryst. Commun.* **2011**, *67*, 871; b) J. Yue, Q. Wang, H. Lu, M. Brennehan, F. Fan, Z. Shen, *Cancer Res.* **2009**, *69*, 7978.
- [23] J.-F. Joanny, J. Prost, *HFSP J.* **2009**, *3*, 94.
- [24] E. J. Young, S. B. Briggs, C. A. Miller, *CNS Neurol. Disord.: Drug Targets* **2015**, *14*, 731.
- [25] a) J. S. Allingham, V. A. Klenchin, I. Rayment, *Cell. Mol. Life Sci.* **2006**, *63*, 2119; b) A. L. Risinger, L. Du, *Nat. Prod. Rep.* **2020**, <https://doi.org/10.1039/C9NP00053D>.
- [26] a) E. Cocucci, J. Y. Kim, Y. Bai, N. Pabla, *Clin. Pharmacol. Ther.* **2017**, *101*, 121; b) B. Sarmiento, F. Andrade, S. B. da Silva, F. Rodrigues, J. das Neves, D. Ferreira, *Expert Opin. Drug Metab. Toxicol.* **2012**, *8*, 607.
- [27] a) N. S. Bryce, E. C. Hardeman, P. W. Gunning, J. G. Lock, *Curr. Opin. Chem. Biol.* **2019**, *51*, 40; b) R. Krishnan, J.-A. Park, C. Y. Seow, P. V. S. Lee, A. G. Stewart, *Trends Pharmacol. Sci.* **2016**, *37*, 87.
- [28] a) S. K. Deshmukh, M. K. Gupta, V. Prakash, S. Saxena, *J. Fungi* **2018**, *4*, 77; b) W. Gao, G. Ye, X. Duan, X. Yang, V. C. Yang, *Int. J. Nanomedicine* **2017**, *12*, 1047; c) J. Hwang, M. Yi, X. Zhang, Y. Xu, J. H. Jung, D. Kim, *Oncol. Rep.* **2013**, *30*, 1929; d) N. R. Jog, M. J. Rane, G. Lominadze, G. C. Luerman, R. A. Ward, K. R. McLeish, *Am. J. Physiol.: Cell Physiol.* **2007**, *292*, C1690.
- [29] I. Foissner, G. O. Wasteneys, *Plant Cell Physiol.* **2007**, *48*, 585.
- [30] a) A. Belluati, V. Mikhalevich, S. Yorulmaz Avsar, D. Daubian, I. Craciun, M. Chami, W. P. Meier, C. G. Palivan, *Biomacromolecules* **2020**, *21*, 701; b) M. Garni, S. Thamboo, C.-A. Schoenenberger, C. G. Palivan, *Biochim. Biophys. Acta, Biomembr.* **2017**, *1859*, 619.
- [31] a) H. C. Shum, J.-W. Kim, D. A. Weitz, *J. Am. Chem. Soc.* **2008**, *130*, 9543; b) H. Wang, Y. Liu, Z. Chen, L. Sun, Y. Zhao, *Sci. Adv.* **2020**, *6*, eaay1438; c) Y. Yu, L. Shang, J. Guo, J. Wang, Y. Zhao, *Nat. Protoc.* **2018**, *13*, 2557.